Journal of Alloys and Compounds 480 (2009) 254–258

Contents lists available at ScienceDirect

Journal of Alloys and Compounds

journal homepage: www.elsevier.com/locate/jallcom

Microstructure and properties of AC-HVAF sprayed Ni60/WC composite coating

S.L. Liu*, X.P. Zheng

School of Materials Science and Engineering, Chang'an University, Xi'an 710061, PR China

ARTICLE INFO

Article history:
Received 12 November 2008
Received in revised form 27 January 2009
Accepted 8 February 2009
Available online 21 February 2009

Keywords:
AC-HVAF
Ni60/WC coating
Microstructure
Wear resistance
Corrosion resistance

ABSTRACT

A Ni60/WC coating was deposited on 0Cr13Ni5Mo stainless steel substrate by the actived combustion-high velocity air fuel (AC-HVAF) technique. The structure and morphologies of the Ni60/WC coating were characterized by X-ray diffraction (XRD) and scanning electron microscopy (SEM), and the wear resistance and corrosion resistance were studied. The results showed that the AC-HVAF spraying was seen as the pre-eminent process for the deposition of Ni60/WC coating. Due to low particle heating and high particle velocity in the HVAF process, WC phase remain almost unchanged after spraying. The tribological behaviors were evaluated by using a HT-600 wear test rig. Under the same conditions, the worn volume of 0Cr13Ni5Mo stainless steel was 10.43 times more than that of the coating. The wear mechanism was mainly fatigue wear. A series of the electrochemical tests was carried out in a 3.5 wt.% NaCl solution in order to examine the corrosion behavior. Mechanisms for corrosion resistance were discussed.

1. Introduction

Wear and corrosion resistance of thermally sprayed coatings has been a subject of numerous investigations over the last decades [1–3]. Nickel-base self-fluxing alloys are mainly used in the chemical industry, glass mould industry based, etc., where corrosion resistance is required. The wear resistance of NiCrBSi coatings can be increased by adding different hard precipitates. Tungsten carbide has the high hardness and a certain degree of ductility compared with the other carbides. It is reported that the addition of WC can improve wear resistance [4].

Ni60/WC composite coating having good wear and corrosion resistant has been widely used in numerous industries. Thermal spraying can also deposit wear and corrosion resistant coatings on cheaper substrate. Several studies concerning the characteristics and performance of thermal Ni–WC coatings showing that the general thermal spray techniques limits its application in very high demanding environments [5–8]. The coating layers so attained are not free from pores and show a relatively weak mechanical performance.

In the family of thermal spray techniques, actived combustion-high velocity air fuel (AC-HVAF) technique are comparatively new thermal spraying methods which can produce coatings with low porosity and high bonding strength to the substrates [9–11]. HVAF is a similar spraying process as HVOF, just using air to replace oxygen. Oxygen replaced with air makes HVAF a lower cost alternative to HVOF [12]. Considering that a high particle velocity is expected to produce a dense coating, HVAF is a good candidate to deposit metal ceramic coating [13]. In addition, it is a low temperature spraying process and uses the nitrogen gas to feed and accelerate the powders. Therefore, no oxidation atmosphere exists in the spraying environment, oxidation of the sprayed powders are farthest avoided. These advantages are particularly suitable for spraying WC-based powder [14].

There are few works reported on the preparation and properties of Ni60/WC composite coating. However, the microstructure as well as the properties, needs more work. This is very important to know about the properties of Ni60/WC composite coating. The aim of this work is to prepare Ni60/WC composite coating by AC-HVAF. As well as the existence of WC particles in nickel matrix, the microstructure and properties of Ni60/WC composite coating were studied.

2. Experiments

An available Ni60/WC powder that has a particle size range of 17–65 μm was used as feedstock material. The chemical composition of the powder was detailed in Table 1. Coating was developed with UniqueCoat Intelli-Jet AC-HVAF thermal spray system, onto commercial 0Cr13Ni5Mo stainless steel coupons which had been grit blasted for a period of 60 s with alumina powder using clean, dry compressed air at 700 kPa. Spraying was performed using propane as the fuel gas; nitrogen was used as the powder carrier gas and compressed air jets were used to cool the samples as soon as the surface temperature of the specimens had exceeded 200 °C. The spray parameters were detailed in Table 2. Flat substrates approximately 20 mm × 20 mm × 3 mm were coated using the following

* Corresponding author. Tel.: +86 24 8233 7340; fax: +86 24 8233 7340.
E-mail address: liushenglin@yahoo.com.cn (S.L. Liu).

0925-8388/$ – see front matter.
doi:10.1016/j.jallcom.2009.02.028

Table 1
Chemical composition of Ni60/WC powder (wt.%).

WC	35
C	<1
Si	5
B	3
Cr	13
Fe	6
Ni	Balance

procedure. The coupons were mounted on holders placed on the circumstance of a turnable, which had a vertical axis of rotation and which was rotated at 120 rpm to give an effective horizontal traverse rate across the spray path 1 m/s. The AC-HVAF gun was placed in front of the coupons at a stand-off distance of 150 mm to give a horizontal spray jet and scanned vertically at 0.005 m/s. All the process parameters, including the spray distance, were kept constant throughout the coating process. Air-cooling of the specimens was employed as soon as the surface temperature of the specimens had exceeded 200 °C.

X-ray diffraction (XRD) of powder and as-sprayed coating was performed on a MXP21VAHF X-ray diffractometer (MAC Science Corp., Japan). X-ray diffraction was done at a tube voltage of 40 kV and a tube current of 200 mA. A small amount of sample was spread evenly in the sample holder. The X-ray intensity was measured over a diffraction angle from 10 to 90° with a velocity of 0.02 per step. Coating morphologies were investigated using SEM (LEO 1450, LEO Corp., UK) with EDS. Microhardness tests were performed using a Digital Micro hardness Tester HXD-1000TM (Shanghai Photics Instrument Co., Ltd., China) with a 300 gf load and a dwell time of 15 s. The particle size distribution of the feedstock was determined by Laser Micronsizer (LMS-30, Seishin Enterprise Co., Ltd., Japan).

A friction and wear test was carried out using a ball-on-disc arrangement on a HT-600 tribometer (Zhongke Kaihua Science and Technology Co., Ltd., China). The ball samples were 6 mm in diameter Si_3N_4 balls. Prior to the friction and wear tests, the coating was ground using diamond sandpaper and then polished using diamond slurries. The experiments were performed under the following conditions: 300 °C, air environment, applied load of 1700 g and sliding velocity of 60 mm/s. During the test, the friction forces were directly measured with a sensor and fed into a computer at a frequency of 20 values per min. Both ball and disc samples were cleaned with ethanol and dry compressed air before and after testing. The friction force data were simply divided by the applied loads to give the friction coefficients. In addition, the worn surfaces were observed with a SEM with EDS to investigate wear mechanisms.

The room temperature electrochemical behavior was examined in the 3.5 wt.% NaCl solution with the potentiostat/galvanostat facility (CHI660B, Shanghai Chenghua Instrument Co., Ltd., China). In the electrochemical tests, the saturated calomel electrode (SCE) and the platinum mesh were used as a reference electrode and a counter electrode, respectively. The electrochemical tests included the open circuit potential measurement, and the potentiodynamic test. The open circuit potential was measured after 30 min immersion of the coating layers in the solution for potential stabilization. The potentiodynamic test was performed at a scanning rate of 2 mV/s.

Table 2
Spray parameters employed for HVAF coating deposition.

Air press/MPa	0.7
Fuel 1 press/MPa	0.52
Fuel 2 press/MPa	0.27
Spraying distance/mm	150
Sending velocity of powders/(g/min)	70

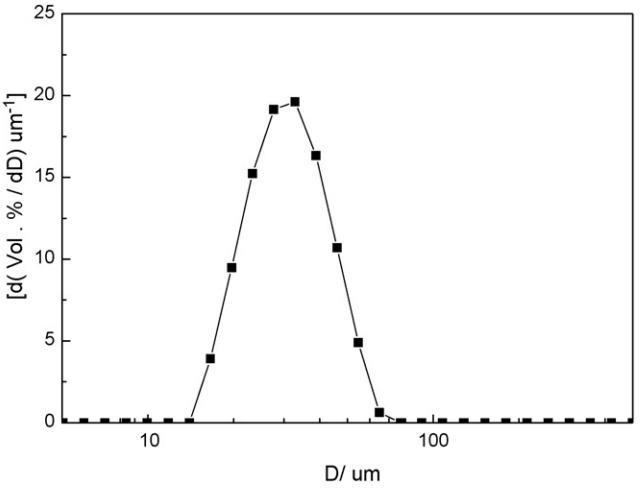

Fig. 1. The particle size distribution of the Ni60/WC composite powder sample as [d(vol.%)/dD] – D curves (D: particle diameter; vol.%: volume percentage).

3. Results and discussion

The particle size distribution for the Ni60/WC powder was examined. The results for the sample Ni60/WC powder was plotted in Fig. 1, as derivative [d(vol.%)/dD – D] curve, which reveal the particle sizes in Ni60/WC powder change roughly between 17 and 65 μm.

Fig. 2 shows the XRD patterns of the Ni60/WC composite powder and AC-HVAF-sprayed coating. Besides the main Cr_2Ni_3 and Ni_4W phase, powder contains some WC phase. The coating predominately consisted of Cr_2Ni_3 and Ni_4W phase, but very weak diffraction peaks of W_2C phase could be detected. It is also shown that there are no new phases formed in the coating during the thermal spray process. It has been revealed that a reduction in flame temperature for thermal spraying led to a decrease in the extent of decomposition of the WC phase.

Compared with powder, all diffraction peaks of the coating are broadened and weakened. X-ray diffraction peaks broaden when the crystal lattice becomes imperfect. The microstructure means the extent and the quality of lattice imperfectness. According to the theory of kinematical scattering, X-ray diffraction peaks broaden either when crystallites become smaller than about a micrometer

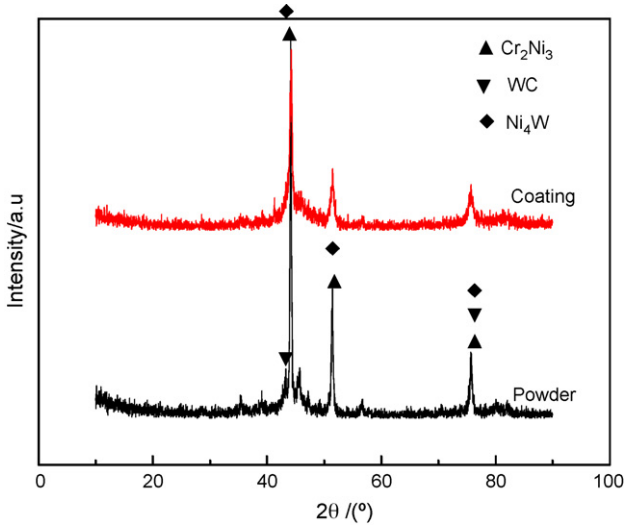

Fig. 2. XRD spectra of the Ni60/WC composite powder atomized powder and AC-HVAF-sprayed coating.

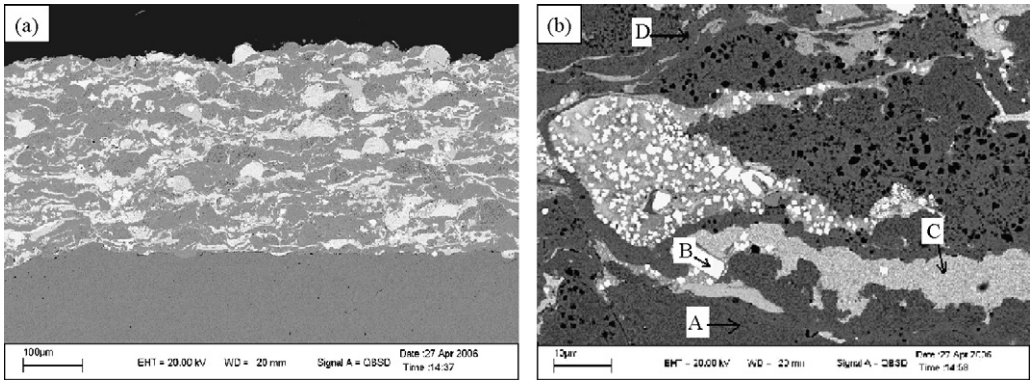

Fig. 3. SEM-back scattered electron images showing cross-sectional microstructures of the Ni60/WC composite coating: (a) low magnification micrographs; (b) high magnification micrographs.

Table 3
Results of the EDS test of different area in Fig. 3.

Zone	Element			
	Cr (wt.%)	Fe (wt.%)	Ni (wt.%)	W (wt.%)
(A) Gray	12.5147	19.7121	62.3983	5.3749
(B) White	2.4950	6.9296	16.7413	73.8341
(C) Weak gray	9.2311	21.6982	48.7302	20.3405
(D) Black	70.3621	13.7361	11.4081	4.4937

or if lattice defects are present in large enough abundance during the thermal spray process [15].

The reasons for amorphous in coatings are mainly associated with two aspects. Firstly, addition of boron is found to be very effective for depressing the melting temperature and increasing the glass-forming ability (GFA) of Ni-based glassy alloys through the increase in the stability of supercooled liquid against crystallization. Secondly, the HVAF spraying is a rapidly heating and cooling process.

Fig. 3 reveals the microstructure of the Ni60/WC coating by SEM. The cross-sectional micrograph with a low magnification (the left side of Fig. 3) revealed a good adhesion between the coating layer and the substrate for the specimens. The high velocity impact of semi-molten coating materials to the substrate accompanies severe plastic deformation and rapid solidification, therefore thermal spray coating layers are likely to possess inevitable pores and microcracks [16]. It is not difficult to be found that the Ni60/WC composite coating is not uniform in the microstructure. The Ni60/WC coating layer exhibited the areas with gray contrast, black contrast, weak gray contrast and white contrast.

The results of EDS analysis was shown in Table 3. As shown in Fig. 3(b), the black area (D) was the Cr rich area a small amount of Fe, Ni, W, and the white area (B) was the W rich area, the gray area (A) was Cr rich area, the weak gray area (C) was Ni, W, Fe rich area.

Table 4 presents the results of porosity in terms of the area fraction of pores, microhardness. The porosity measurements were made with image analyser, having software of Dewinter Material Plus 1.01 based on ASTM B276. The porosity of the coatings is in good agreement with their microstructure as shown in Fig. 2. It is easy to be seen that the coating has few porosity.

In earlier studies, the Ni60/WC powder coatings showed the high amount of porosity [5–7,17]. However, in the present case of AC-HVAF sprayed Ni60/WC coating, the porosity is found to be negligible (Fig. 3). Producing a dense coating can be attributed to a high particle velocity during the AC-HVAF thermal spray.

Table 4
Summary of coating properties.

Coating properties	Data
Porosity (%)	1.3
Microhardness (HV300)	1275

The microhardness of the AC-HVAF coating is high. Similar studies showed that the microhardness of Ni60/WC powder coatings is only about HV800 [17–19]. However, in the present case of AC-HVAF sprayed Ni60/WC coating, the microhardness is 1275 ± 80. This can be attributed to two roles. The first is that it can reduce the decarburization of WC during AC-HVAF spray process. The second is that it contributes to a high particle velocity during AC-HVAF spraying, after high-speed particles sprayed onto the matrix, the strong deformation reinforcement is produced.

The variation in coefficient of friction with time for the Ni60/WC coating is presented in Fig. 4. The variation of coefficient of friction data is somewhat large. During the initial stages of the Ni60/WC coating corresponded to a time of approximately 60 s, the value of the coefficient of friction sharply increased due to highly adhesive micro-contacts between the mating surfaces. The Ni60/WC coating shows a better wear resistance than the 0Cr13Ni5Mo stainless steel. The Ni60/WC coating shows the lower wear volume of 9.42×10^{-3} mm than the 0Cr13Ni5Mo stainless steel 98.31×10^{-3} mm. The wear volume of the 0Cr13Ni5Mo stainless steel was 10.43 times than that of the Ni60/WC coating.

Fig. 5 shows the SEM micrographs of the worn surfaces of the Ni60/WC coating. Fig. 5(a) shows the wear scars on the coating. Some dark regions appear in the wear region. According to the higher magnification plan view of the wear track (Fig. 5(b)), it is not difficult to see that the wear track on the coating exhibited

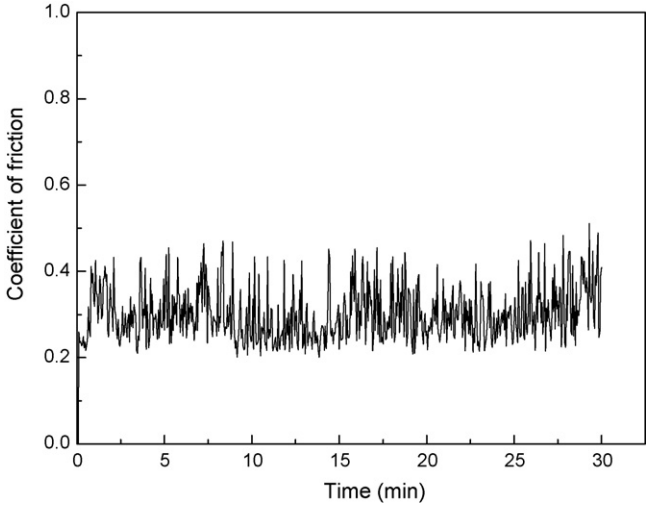

Fig. 4. Friction coefficient of the Ni60/WC coating.

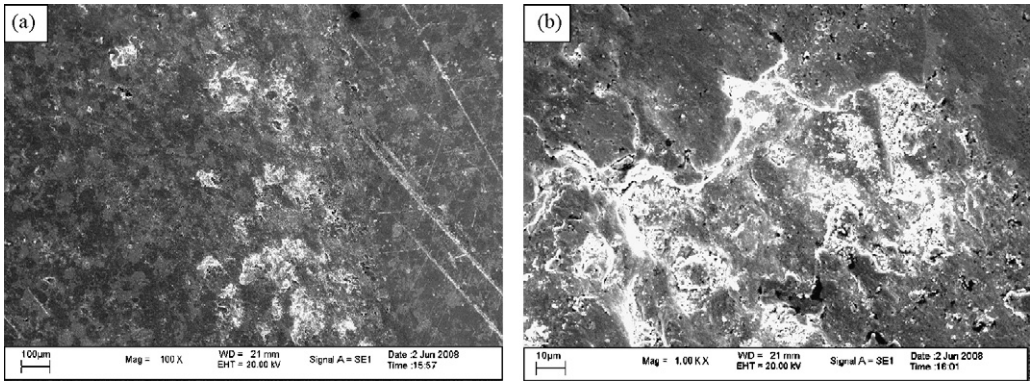

Fig. 5. SEM micrographs of the worn surfaces of the Ni60/WC coating.

small amount of material removal from the wear track. Further, less spallation and fracturing of lamellae can be found on the coating. In addition, there appear some little holes and cracks in the dark regions (Fig. 5(b)). From the worn features, it can be seen that the wear mechanisms of the coating produced using mechanically milled powder is adhesion-induced spallation and fracturing of lamellae.

The open circuit potential values of the constituents of both substrate and coating materials measured after 30 min immersion in the 3.5 wt.% NaCl solution were plotted in Fig. 6. The open circuit potential of coating was much higher than that of 0Cr13Ni5Mo stainless steel. It is anticipated that this fact may affect significantly the corrosion behavior of the coating layers in two ways. First, the open circuit potential difference between WC particles and binder materials causes the microgalvanic corrosion between them in the NaCl environment. The WC becomes cathodic and the binder material becomes anodic, resulting in corrosion of anodic binder materials. Second, the substrate material exhibits lower potention [20]. When the NaCl solution infiltrates along the microcracks existing at the coating layer/substrate interface, the macrogalvanic corrosion is likely to occur at the interface [21].

Fig. 7 displays the potentiodynamic polarization curves of the Ni60/WC coating, in comparison with the corresponding Ni60/WC coating and stainless steel substrate (0Cr13Ni5Mo) in 3.5 wt.% NaCl solution. The Ni60/WC coating exhibits excellent corrosion resistance indicated by the extremely low passive current density and wide passive region. The 0Cr13Ni5Mo stainless steel is passivated with a higher passive current density after a section of active solution, indicating its inferior corrosion resistance to that of the Ni60/WC coating.

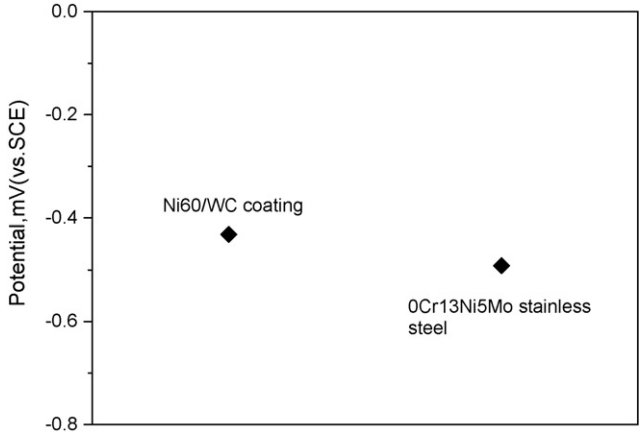

Fig. 6. Comparison of the open circuit potential of the constituents of coating materials and substrate in the 3.5 wt.% NaCl solution.

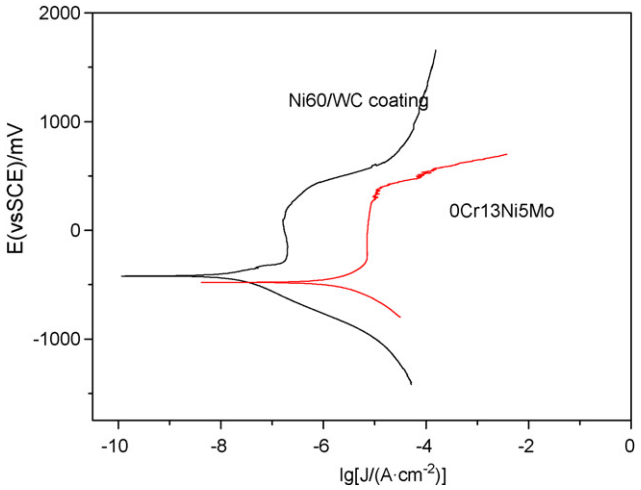

Fig. 7. Potentiodynamic polarization curves of the present coating layers in the 3.5 wt.% NaCl solution.

Generally, the corrosion potential of the coating layer was higher than that of the 0Cr13Ni5Mo stainless steel due to the passive film forming effect of Cr [21]. As shown in Fig. 7, the whole curves can be divided into the two regions. In region I (the potential < 270 mV), the current density of the coating layers exhibited the initial exponential increase with increasing the potential and then remained nearly unchanged with the further potential increase.

The region I behavior of the 0Cr13Ni5Mo stainless steel is the typical passive behavior. Although the region I of the Ni60/WC coating behavior is similar to the general passive behavior, it is different from the general passivity.

In region II (the potential > 270 mV), the coating layer and 0Cr13Ni5Mo stainless steel exhibited the rapid increase of the current density with increasing the potential, similar to the typical trans-passive behavior.

The corrosive behavior of the Ni60/WC coating in NaCl fog environment was investigated so as to study the corrosion resistance of the Ni60/WC coating. The Ni60/WC coating shows the longer time of first rust of 144 h than the 0Cr13Ni5Mo stainless steel 12 h. The time of first rust of the Ni60/WC coating was 12 times than that of the 0Cr13Ni5Mo stainless steel.

4. Conclusions

(1) The Ni60/WC coating has the dense coating structure, and exhibits the less pores and interlamellar and intralamellar cracks.

(2) The lower temperature of spraying flame can diminish WC dissolution in the binder, it is effective in retarding decarburization. The excellent wear properties of the Ni60/WC coating were tested under sliding against Si_3N_4 ball.
(3) The corrosion potential of the coating layer was higher than that of the 0Cr13Ni5Mo stainless steel due to the passive film forming effect of Cr. The Ni60/WC coating produced by AC-HVAF spraying enabled to improve the corrosion resistance of the 0Cr13Ni5Mo stainless steel.

References

[1] A.C. Savarimuthu, H.F. Taber, I. Megat, J.R. Shadley, E.F. Rybicki, W.C. Cornell, W.A. Emery, D.A. Somerville, J.D. Nuse, J. Therm. Spray Technol. 10 (2001) 502.
[2] L. Jacobs, M.M. Hyland, M. De Bonte, J. Therm. Spray Technol. 8 (1999) 125.
[3] W.M. Zhao, Y. Wang, L.X. Dong, K.Y. Wu, J. Xue, Surf. Coat. Technol. 190 (2005) 293.
[4] H. Wang, W. Xia, Y. Jin, Wear 195 (1996) 47.
[5] M.P. Planche, H. Liao, B. Normand, C. Coddet, Surf. Coat. Technol. 200 (2005) 2465.
[6] S. Stewart, R. Ahmed, T. Itsukaichi, Surf. Coat. Technol. 190 (2005) 171.
[7] J. Rodríguez, A. Martín, R. Fernández, J.E. Fernández, Wear 255 (2003) 950.
[8] R. McPherson, Surf. Coat. Technol. 39 (40) (1989) 173.
[9] D.W. Parker, G.L. Kutner, Adv. Mater. Process 139 (1991) 68.
[10] G. Davies, M. Breitsameter, Weld. Res. Abroad 43 (1997) 5.
[11] R. Thorpe, H. Kopech, N. Gagne, Adv. Mater. Process 157 (2000) 27.
[12] A.P. Wang, Z.M. Wang, J. Zhang, J.Q. Wang, J. Alloys Compd. 440 (2007) 225.
[13] A.P. Wang, X.C. Chang, W.L. Hou, J.Q. Wang, Mater. Sci. Eng. A, Struct. Mater.: Propert. Microstruct. Process. 449–451 (2007) 277.
[14] S. Liu, D. Sun, Z. Fan, H.-y. Yu, H.-m. Meng, Surf. Coat. Technol. 202 (2008) 4893–4900.
[15] T. Ungar, Scripta Mater. 51 (2004) 777–781.
[16] H.L. de Villiers Lovelock, P.W. Richter, J.M. Benson, P.M. Young, J. Therm. Spray Technol. 7 (1998) 57.
[17] M.J. Tobar, C. Álvarez, J.M. Amado, G. Rodríguez, A. Yáñez, Surf. Refs. [17] and [20] are similar, hence Ref. [20] has been deleted from the list and subsequent references have been renumbered accordingly in both text and list. Please check.Coat. Technol. 200 (2006) 6313–6317.
[18] W.-M. Song, G.-R. Yang, J.-J. Luc, Y. Hao, Mater. Sci. Eng. A 445–446 (2007) 537–542.
[19] Z. Liu, J. Cabrero, S. Niang, Z.Y. Al-Taha, Surf. Coat. Technol. 201 (2007) 7149–7158.
[20] T. Hodgkiess, A. Neville, An Assessment of Galvanic Effects in Thermal Sprayed Coating System. A United Forum for Scientific and Technological Advances, ASM International, OH, USA, 1997, p. 167.
[21] J.E. Cho, S.Y. Hwang, K.Y. Kim, Surf. Coat. Technol. 200 (2006) 2653.